A FINITE ELEMENT APPROACH FOR MODELING DYNAMIC EFFECTS OF PRESTRESSING IN CONCRETE BEAMS

Andressa Bianco Estruzani[a] https://orcid.org/0009-0007-2356-5388, **Aref Kalilo Lima Kzam[b]** ORCID, **Jesús Daniel Villalba-Morales[c]** https://orcid.org/0000-0001-8339-2262, **Iván Darío Gómez Araujo[b]** https://orcid.org/0000-0001-7088-8322

[a]Department of Civil Engineering, University Center Dinâmica das Cataratas, Foz do Iguaçu, PR, Brazil. Email: andressa.bianco@udc.edu.br

[b]Department of Civil Engineering, Federal University for Latin American Integration – UNILA, Foz do Iguaçu, PR, Brazil. Email: aref.kzam@unila.edu.br，ivan.araujo@unila.edu.br

[c]Department of Civil Engineering, Pontificia Universidad Javeriana, Bogota, DC, Colombia. Email: jesus.villalba@javeriana.edu.co

*Corresponding author

Abstract

Prestressed concrete structures are widely utilized in civil engineering due to their superior structural efficiency and load-carrying capacity. However, long-term losses in prestressing force can compromise both structural integrity and service performance. This study presents a finite element-based numerical model developed to assess the impact of prestressing force on the natural frequencies of simply supported beams. The model accounts for the combined effects of axial compression and the physical characteristics of the tendon, including variations in eccentricity and geometric profile, on the dynamic response of the structure. Validation against experimental results reported in the literature demonstrates strong correlation, particularly for the first and second vibration modes, with average discrepancies of 2.48% and 2.68%, respectively. Numerical simulations also reveal that the influence of prestressing is most pronounced during the early stages of loading, with frequency shifts tending to stabilize as the applied load nears critical levels. The proposed dynamic analysis framework offers a valuable complementary approach for the indirect estimation of prestress losses, thereby improving the precision and effectiveness of structural health monitoring and maintenance strategies in prestressed concrete systems.

Keywords

Prestressed concrete, Modal analysis, Finite Element Method, Structural dynamics, Monitoring

Graphical Abstract

Problem: Prestressed Beam

Optimization: Genetic Algorithm

Results: FEM vs EXP
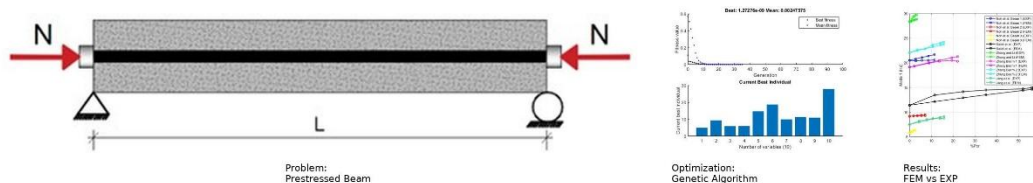
1 INTRODUCTION

Since its introduction in the 1930s, prestressed concrete has revolutionized structural engineering, becoming one of the most versatile and efficient construction methods for large-scale structures (Zhao and Fang 2012). This technique involves inducing pre-compressive stresses in concrete through tensioned steel tendons, thus counteracting the tensile stresses resulting from external loads (Shi, He, and Yan 2014). This fundamental principle offers significant advantages over conventional reinforced concrete, which suffers from stress from tension. In that sense, its application extends from precast elements, such as beams and slabs, to complex structures, including long-span bridges, high-rise buildings, and reservoirs (Breccolotti 2018). Among the main benefits of prestressing are effective crack control, reduced long-term deformations, and increased load-bearing capacity of structural elements (H.-T. Kim, Seo, and Yang 2019). In addition, it enables the development of more slender and lightweight structures, with significant material savings, without compromising safety or durability. In addition, prestressing contributes to the rationalization of construction, allowing longer spans and more ambitious architectural solutions (Choudhary and Sanghai 2019). From a sustainability perspective, prestressed and precast systems contribute to increased energy efficiency and reduced embodied energy (Fleischman and Seeber 2016). Further performance improvements can be achieved through the application of optimization techniques in the design of prestressed elements, as demonstrated in recent studies (Amir and Shakour 2018; Jahjouh and Erhan 2022; Shakur, Shaked, and Amir 2024).

One of the critical challenges in the use of prestressed concrete is the progressive loss of prestressing force over time. Phenomena such as creep and shrinkage of concrete, steel relaxation, reinforcement corrosion, and thermal variations can significantly reduce system efficiency (Zanini, Faleschini, and Pellegrino 2022). In this context, the non-destructive assessment of the prestress state has become critical for the maintenance and safety of prestressed structures. To this respect, techniques based on dynamic parameters, particularly the analysis of natural vibration frequencies, have gained attention as promising alternatives for estimating prestress losses (Ribeiro et al. 2021; L. Wang, Li, and Xu 2020). Natural frequencies are highly sensitive to changes in global stiffness, which in turn is influenced by variations in the prestressing force (Saiidi, Douglas, and Feng 1994; Zhou, Li, and Zhang 2020). An example is the work by Kovalovs (Kovalovs et al. 2017), who proposes a method based on dynamic vibration monitoring, implemented through finite element analysis, and validated by comparison with experimental data. Recent advances, such as machine learning techniques (Ribeiro et al. 2021), enhanced modal identification methods (L. Wang, Li, and Xu 2020), and smart monitoring systems (Liu et al. 2022; Bao et al. 2021), have further expanded the potential for dynamic-based prestress evaluation. It should be noted that monitoring of dynamic parameters has also been used as a tool to verify the safety and integrity of structures, since these parameters are directly related to stiffness, mass, boundary conditions, and, consequently, to structural deterioration and/or cracking (Saidin et al. 2022). It is worth mentioning that Abdel-Jaber and Glisic (2019) present a review on monitoring of prestressing forces, which includes vibration methods, impedance-based methods, elasto-magnetic methods, acoustoelastic methods, and strain-based methods. In addition, Bonopera et al. (Marco Bonopera, Chang, and Lee 2020) carried out a state-of-the-art on the subject with application to prestressed concrete girders and static-based methods.

However, it is important to note that the understanding on how prestressed force affects the dynamic behavior – and consequently on natural frequencies – of prestressed beams is yet a topic of disagreement among various authors in the literature (Noble et al. 2014). In theoretical studies grounded in classical mechanics, the vibration analysis of beams subjected to axial loads is a well-established topic in technical publications. Several authors (Shaker 1975; Bokai 1988; Mamandi, Kargarnovin, and Farsi 2012) have assumed that the prestressing force in the tendon is equivalent to an axial compressive load. In this approach, natural frequencies tend to decrease with increasing compressive force due to the so-called "compression softening" effect, as predicted in Euler–Bernoulli beams (M. Bonopera et al. 2019). On the other hand, Hamed and Frostig (2006) argue that the natural frequencies of the structural elements are not affected by the prestressing force. This argument is based on a nonlinear kinematic model which concludes that the final dynamical equation of motion for a prestressed beam is independent of the magnitude of the prestressed force. An alternative methodology that has been used is the development of physical models in laboratory settings. Various experimental studies conducted on prestressed concrete beams, such as those of references (Saiidi, Douglas, and Feng 1994; Noh et al. 2015; Y. Zhang and Li 2007; Y. T. Zhang, Zheng, and Li 2011; Jang et al. 2011), have shown an increasing trend in natural frequencies with higher levels of prestressed force, contradicting theoretical studies that claim otherwise. Moreover, Risan and Zaki (2022) elaborated a meta-analysis on the subject, finding that the statistical results support the feasibility of using the change in the natural frequency for the fundamental mode in the process of determining the prestress losses.

Given the inherent complexity of modeling the dynamic behavior of prestressed structures, this study proposes a finite element modeling approach for analyzing prestressed concrete beams. This approach considers both experimental results from literature and a metaheuristic algorithm for model updating. The main contributions of this paper are as follows:

- The development of a finite element modeling approach that is capable of simultaneously considering the effects of axial compression and the structural contribution of the physical presence of tendons to the global stiffness of prestressed beams. The proposed model allows for the analysis of beams with curved tendons and eccentricities, which are typical of real-world structures such as bridges and viaducts and are often neglected in previous studies.

- A comprehensive review of the main theoretical and experimental studies available in the literature to support the formulation and validation of the proposed model. This validation is conducted using a genetic algorithm, where the objective function minimizes the error between experimental and analytical natural frequencies of the beams prior to the application of prestressing.

- The quantification of the relationship between the natural frequencies of the beam and the level of prestressing load. Visual representations and tables are provided to facilitate the interpretation of the results.

2 LITERATURE BACKGROUND

Despite significant research efforts, the influence of prestressing force on the natural frequencies of concrete beams remains a controversial topic. Discrepancies between theoretical predictions and experimental observations have been consistently reported, leading to the development of a variety of analytical, numerical, and experimental studies to better understand this phenomenon. A brief review of the main contributions on this topic is presented below, including theoretical investigations and experimental tests.

2.1 Theoretical Research

The presence of an axial force in a homogeneous beam alters its natural vibration frequencies, a phenomenon resulting from the effect known as "compression softening," which is described by the classical Euler-Bernoulli model (Noh et al. 2015). For a simply supported prismatic beam, as illustrated in Figure 1, the equilibrium equation, considering the boundary conditions, leads to the following equation for the natural frequency:

$$\omega_n^2 = -\left(\frac{n\pi}{L}\right)^2 \frac{N}{m} + \left(\frac{n\pi}{L}\right)^4 \frac{EI}{m} \tag{1}$$

where ω_n is the natural frequency, n is the mode number, L is the length of the beam, N is the axial compressive force, E is the modulus of elasticity, I is the moment of inertia and m is the mass per unit length. As can be seen, the natural frequencies depend on the magnitude of the prestressed load. However, such an expression cannot be straightforwardly obtained for other conditions. For more complex structures, it is necessary to employ the finite element method (FEM) to describe the relationship between the characteristics of the prestressed beam and its dynamic characteristics. There are several aspects to consider, including the boundary conditions, the prestressed force magnitude, geometric non-linear behavior, and the load eccentricity.
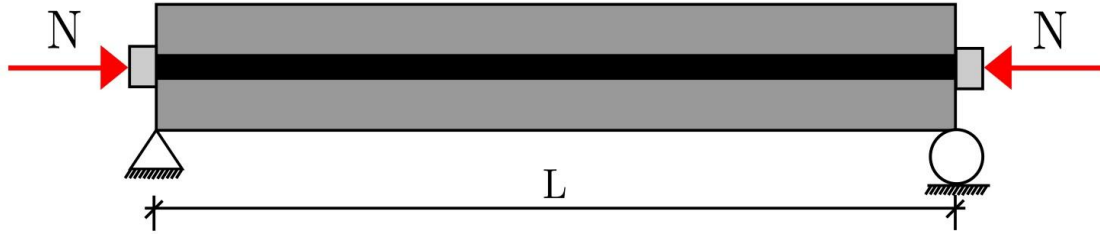
Figure 1 Model of a prestressed beam

In the literature, several studies on the subject have focused on the impact of the prestressed load on the dynamics characteristics of beam-type concrete elements. The first studies in the decades of the 70s (Shaker 1975) and 80's (Bokaian 1988; Raju and Rao 1986) pointed out the effect of increasing the axial prestressed load (prestress) on the decrement of natural frequencies of beams with different boundary conditions, especially for the fundamental and lower modes. Law and Lu (2005) analyzed the time domain response of an Euler-Bernoulli prestressed concrete beam subjected to axial compression, concluding that the lower natural frequencies were most affected by axial compression due to the compression softening effect. In addition, references (Miyamoto et al. 2000; J.-T. Kim, Ryu, and Yun 2003; Jaiswal 2008; Vibhute et al. 2016) found numerically that all natural frequencies in beams exhibited a decreasing trend. Bai-Jian, Fei, and Song (2018) studied the influence of the prestressing force, eccentricity, and cross-sectional area on simply supported steel beams and concluded that prestressing does not affect the even-order frequencies, but the odd-order frequencies decrease with increasing prestressing force. Furthermore, frequencies increase with eccentricity and cross-sectional area. In contrast, Kim proposed an alternative model that showed an increase in natural frequency with the prestressing force, particularly in the first modes, which was confirmed by experimental tests performed by Saiidi, Douglas, and Feng (1994). Hamed and Frostig (2006) in a non-linear geometric model, proposed that the prestressing force does not affect the natural frequency, justified by the ideal condition of the adhesion of the cable to the concrete. However, this model was not experimentally verified. Gan et al. (2019) conducted numerical simulations using the Finite Element Method to investigate the effect of the prestressing force on natural frequencies, considering microcracks caused by concrete shrinkage. The results showed that the prestressing force tends to close these cracks, increasing rigidity and consequently increasing natural frequency.

As can be seen in the previous paragraphs, theoretical studies suggest that the prestressing force, when considered as an external axial load, decreases the natural frequencies. However, some experimental studies suggest that prestressed beams do not have a significant effect on the natural frequencies of prestressed beams. The discrepancy between theories and experimental results suggests the need for more in-depth investigations, particularly in the experimental field, to confirm the observed trends. Additionally, the physical presence of the prestressed cable may generate internal forces that increase the beam's rigidity, resulting in a trend contrary to theoretical predictions.

2.2 Experimental Research

From an experimental point of view, several studies have tried to reproduce in the laboratory the real condition of the prestressed elements in the field to more accurately determine the relationship between presstress forces and the dynamic parameters of the beam. Hop (1991) and Saiidi, Douglas, and Feng (1994) demonstrated that, for beams with straight concentric cables, the natural frequency increases with increasing prestressing force, contradicting theoretical predictions that treat prestressing as an axial compressive force. J.-T. Kim, Ryu, and Yun (2003) proposed an analytical model, which, compared to the results of Saiidi, Douglas, and Feng (1994), also found a tendency for the natural frequency to increase. However, some explanations have been proposed to justify these discrepancies. Saiidi, Douglas, and Feng (1994) suggested that the differences between the experimental values and those predicted by classical theories could be attributed to the presence of microcracks, which close when the prestressing force is applied, thus increasing the stiffness of the beam and, consequently, its natural frequency. This hypothesis is based on Equation (2), which proposes an empirical formula for the effective stiffness $(EI)_e$, given by:

$$(EI)_e = \left(1 + 1.75 \frac{N}{f_c'}\right) EI_g \tag{2}$$

where N is the applied axial force, f_c is the compressive strength of the concrete at 28 days, and EI_g is the stiffness of the beam without prestressing. Although this formula is widely used, Bai-Jian et al. (2018) highlight that it lacks complete theoretical support.

Subsequent studies, such as those of Dall'Asta and Dezi (1996) and Deak (1996), followed similar approaches but with contradictory results. Although Dall'Asta and Dezi concluded that the natural frequency was not significantly affected by the prestressing force, Deak attributed the frequency variation to the formation and closure of microcracks due to the shrinkage of the concrete prior to the application of prestressing.Jain and Goel (1996) discussed that the prestressing force does not affect the natural frequency because the cable becomes an integral part of the system. Other studies, such as those of Miyamoto et al. (2000), observed a decrease in natural frequency as the prestressing force increased in beams with external prestressing, although this trend was not observed in models with more eccentric cables. Other authors, such as Lu and Law (2006), proposed a numerical model based on Euler-Bernoulli theory and observed that for centralized straight cables, the natural frequencies increased with increasing prestressing force, again contradicting theoretical predictions. Y. Zhang and Li (2007) found the same trend in their experiments. Furthermore, Jang et al. (2011) validated a numerical model with Equation ([Eq2]) and observed a progressive increase in frequency with the increase in prestressing force.

In contrast to these results, some authors, such as (T. Wang, Huang, and Wang 2013), used the Rayleigh method to study the natural frequency in prestressed concrete beams with straight and parabolic cables. For parabolic cables, the frequency decreased with the prestressing force, while for straight cables, the frequency was unaffected. Shi, He, and Yan (2014) observed that the lower order frequencies increased with increasing prestressing force, which corroborates the findings of Saiidi, Douglas, and Feng (1994). More recent studies, such as those by Noble et al. (2016), found no clear relationship between prestressing force and natural frequency, observing that the trend was inconsistent. However, Noh et al. (2015) performed tests on models with different eccentricities and observed that for models with eccentric cables, the natural frequency increased with increasing prestressing force. Furthermore, Li and Zhang (2016) conducted a study that combined experimental tests and numerical simulation, concluding that the relationship between prestressing force and natural frequency cannot be explained by traditional theory but by a more complex model that considers cable eccentricity. Finally, M. Bonopera et al. (2019) performed laboratory tests on beams with a parabolic cable profile and found that natural frequency was not affected by the prestressing force. These results reinforce the idea that there is no consensus on the influence of the force, eccentricity, and cable profile of the prestressed concrete beams.

In summary, most studies suggest that an increase in prestressing force tends to increase the natural frequency of prestressed concrete beams, although considerations of the presence of microcracks and cable eccentricity may influence this behavior. However, as highlighted by Noh et al. (2015) and others, the relationship between these parameters still needs to be better understood.

3 PROPOSED FINITE ELEMENT MODELING

This research proposes a one-dimensional finite element modeling strategy for computing the modal properties of prestressed beams, which accounts for two simultaneous conditions: the axial compression induced by the prestressed force and the internal presence of the tendons, which generate resistance forces that increase the flexural stiffness. It is worth mentioning that the effect caused by the mentioned issues on the dynamic behavior of the prestressed beam is opposite. On the one hand, axial compression tends to reduce the natural frequencies of the beam, while the presence of the tendon contributes to their increase. Thus, the resulting effect will lie at an intermediate point between opposite trends in the dynamic parameters. Identifying the prevailing trend is essential for assessing the sensitivity of dynamic monitoring techniques to prestress losses.

Initially, the effect of axial compression due to the prestressing force will be analyzed, assuming a set of linear variations of the internal axial force along the beam's length. To this end, an equilibrium equation for a beam subjected to axial load will be formulated and numerically solved using the Galerkin method (Cook et al. 2002). Subsequently, the effect of the tendon will be modeled as an equivalent distributed load, corresponding to the resistance moment generated by the prestressing force in the cross section. The stiffness matrix will be formulated on the traditional basis of the variational approach, as described in (Zienkiewicz, Taylor, and Zhu 2013). It is highlighted that the model is computationally efficient as it was kept depending only on the main axis of the beam.

3.1 Analysis Including the Effect of Axial Load

The mathematical model for computing the dynamic characteristics of a prestressed beam was based on the classical Bernoulli beam theory. In that sense, the derivation of the governing equation for the vibratory motion of uniform beams subjected to axial loads is extensively presented in the literature on vibration theory, including the work by Shaker (1975). However, the main limitation of some approaches is related to the fact that the internal axial load is assumed to be constant along the element. This assumption differs from the real condition, as the forces vary for each point on the beam. To solve this situation, it is proposed that the equilibrium equation considers the variation of the axial load along the length of the beam. The beam under study is simply supported, with length L and stiffness EI, subjected to an axial force P of constant magnitude and direction, which is considered positive when acting in compression. Additionally, the beam is subjected to a distributed transverse load applied along its entire length, with continuous positive values when acting downward. Figure 2 illustrates the beam configuration, aligned along the x axis and subjected to the aforementioned loading conditions.
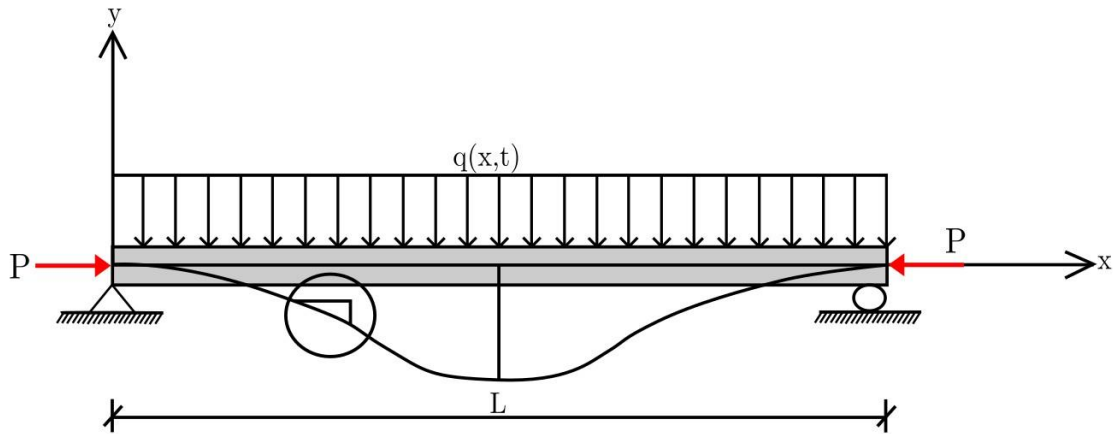
Figure 2 Simply supported beam under axial and transverse loading

From the beam considered, an infinitesimal element of length dx will be isolated to derive the equilibrium equation. This element is subjected to constant axial force P, a distributed transverse load, internal shear forces V and $V + dV$, and bending moments M and $M + dM$. In addition, the inertial forces associated with transverse vibration, represented by $m\,dx\,\ddot{u}$, are taken into account. The configuration of the element and the acting forces is illustrated in Figure 3. Based on the equilibrium of forces and moments and applying the classical Euler-Bernoulli beam theory, the relationships between the bending moment, the shear force, and the transverse displacement of the beam lead, after some algebraic manipulations, to the following expression. Damping is not considered during the formulation.

$$EI\frac{\partial^4 u(x,t)}{\partial x^4} + P(x)\frac{\partial^2 u(x,t)}{\partial x^2} + \frac{dP(x)}{dx}\frac{\partial u(x,t)}{\partial x} + m\frac{\partial^2 u(x,t)}{\partial t^2} = q(x,t) \quad (3)$$
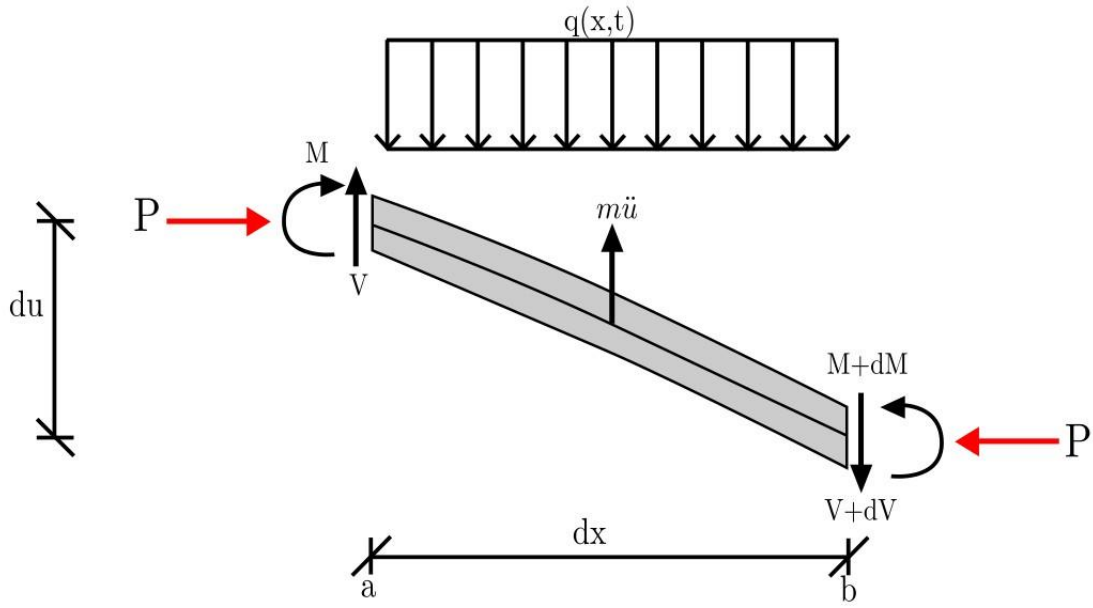
Figure 3 Beam element

Equation (3) is a partial differential equation of fourth order in space and second order in time, derived from the Euler-Bernoulli beam theory and accounting for the influence of a spatially varying axial load. The term m denotes the mass per unit length, defined as $m = \rho A$, where ρ is the density of the material and A is the cross-sectional area of the beam. A numerical solution for the differential equation will be developed using the Galerkin method. The Galerkin method seeks an approximate solution $\tilde{u}(x)$ to the exact solution $u(x)$, generating a residual through the expansion of coefficient-based functions. These residuals must be weighted, and the goal is to minimize them using the following integral (J.-T. Kim, Ryu, and Yun 2003):

$$\int_0^L R\,(x)\phi_i(x)\,dx = 0, \quad i = 1, \dots, N \quad (4)$$

Applying Equation (4) to Equation (3), the following equation is obtained:

$$\int_0^L [EI\,u^{IV} + P\,u'' + P'\,u' + m\,\ddot{u} - q(x,t)]\,\phi_i(x)\,dx = 0 \quad (5)$$

Next, each integral of Equation (5) will be presented individually. Thus, the component related to the elastic forces is:

$$\int_0^L \frac{EI\,\partial^4 u(x,t)}{\partial x^4}\,\phi_i(x)\,dx \quad (6)$$

Using integration by parts twice and applying the boundary conditions for shear and moment, we obtain:

$$-[V(L)\phi_i(L) + V(0)\phi_i(0)] - P(x)\frac{\partial \tilde{u}(x,t)}{\partial x}\phi_i(x)\Bigg|_0^L$$
$$-\left[M(L)\frac{\partial \phi_i(L)}{\partial x} - M(0)\frac{\partial \phi_i(0)}{\partial x}\right] + \int_0^L EI\,\frac{\partial^2 \tilde{u}(x,t)}{\partial x^2}\frac{\partial^2 \phi_i(x)}{\partial x^2}\,dx = 0 \quad (7)$$

In addition, the component related to the forces generated in the flexure raised in the presence of the tendons:

$$\int_0^L P\,(x)\frac{\partial^2 \tilde{u}(x,t)}{\partial x^2}\phi_i(x)\,dx \quad (8)$$

After applying integration by parts, Equation ([Eq6]) becomes:

$$\left[P(x)\frac{\partial \tilde{u}(x,t)}{\partial x}\phi_i(x)\right]_0^L - \int_0^L \frac{\partial P(x)}{\partial x}\phi_i(x)\frac{\partial \tilde{u}(x,t)}{\partial x}dx - \int_0^L P(x)\frac{\partial \phi_i(x)}{\partial x}\frac{\partial \tilde{u}(x,t)}{\partial x}dx \quad (9)$$

Then, the component related to the axial forces due to the prestressed loads:)

$$\int_0^L \frac{\partial P(x)}{\partial x}\frac{\partial \tilde{u}(x,t)}{\partial x}\phi_i(x)\,dx \quad (10)$$

Using integration by parts:

$$\left[\frac{\partial P(x)}{\partial x}\tilde{u}(x,t)\phi_i(x)\right]_0^L - \int_0^L \frac{\partial P(x)}{\partial x}\frac{\partial \phi_i(x)}{\partial x}\tilde{u}(x,t)dx - \int_0^L \frac{\partial^2 P(x)}{\partial x^2}\phi_i(x)\tilde{u}(x,t)dx \quad (11)$$

To analyze the beam, an approximate function for the displacement field is required that describes the deformed configuration under nodal displacements. This function is given in the following, considering the displacement and rotation boundary conditions at nodes i and j:

$$\tilde{u}(x) = \mu_i\phi_1(x) + \mu_{i'}\phi_2(x) + \mu_j\phi_3(x) + \mu_{j'}\phi_4(x) = \{\phi(x)\}\{\delta\}^T \tag{12}$$

where the shape functions are:

$$\begin{cases} \phi_1(x) = 1 - 3\left(\frac{x}{L}\right)^2 + 2\left(\frac{x}{L}\right)^3 \\[2mm] \phi_2(x) = x - \frac{2x^2}{L} + \frac{x^3}{L^2} \\[2mm] \phi_3(x) = 3\left(\frac{x}{L}\right)^2 - 2\left(\frac{x}{L}\right)^3 \\[2mm] \phi_4(x) = \frac{x^3}{L^2} - \frac{x^2}{L} \end{cases} \tag{13}$$

Furthermore, it is assumed that the prestressing force is linearly varied between nodes i and j, according to:

$$P(x) = p_i + \frac{p_j - p_i}{L}x \quad (14)$$

Substituting the approximation function (Eq. 10) and the prestress function (Eq. 12) in Equations (5), (7) and (9), the stiffness and geometric matrices for the beam under variable axial load can be obtained. The last integral in Equation (5) yields the elastic stiffness matrix:

$$[K_e] = \int_0^L E\,I\phi_{j''}(x)\phi_{i''}(x)dx \quad (15)$$

which can be written in matrix form as:

$$[K_e] = \frac{EI}{L^3}\begin{bmatrix} 12 & 6L & -12 & 6L \\ 6L & 4L^2 & -6L & 2L^2 \\ -12 & -6L & 12 & -6L \\ 6L & 2L^2 & -6L & 4L^2 \end{bmatrix} \quad (16)$$

From equations (7) and (9), the geometric stiffness matrix is defined as follows:

$$[K_{g1}] = \int_0^L P(x)\phi_{i'}\phi_{j'}dx + \int_0^L P'(x)\phi_i\phi_{j'}dx + \int_0^L P'(x)\phi_{i'}\phi_j dx \quad (17)$$

The sum of these three integrals yields the geometric matrix:

$$[K_{g1}] = \begin{bmatrix} \dfrac{3}{5} \cdot \dfrac{p_j + p_i}{L} & \dfrac{1}{10}p_j & -\dfrac{3}{5}\dfrac{(p_j + p_i)}{L} & \dfrac{1}{10}p_i \\[2mm] \dfrac{1}{10}p_j & \dfrac{1}{30}Lp_j + \dfrac{1}{10}Lp_i & -\dfrac{1}{10}p_j & -\dfrac{1}{60}Lp_j - \dfrac{1}{60}Lp_i \\[2mm] -\dfrac{3}{5}\dfrac{(p_j + p_i)}{L} & -\dfrac{1}{10}p_j & \dfrac{3}{5} \cdot \dfrac{p_j + p_i}{L} & -\dfrac{1}{10}p_i \\[2mm] \dfrac{1}{10}p_i & -\dfrac{1}{60}Lp_j - \dfrac{1}{60}Lp_i & -\dfrac{1}{10}p_i & \dfrac{1}{10}Lp_j + \dfrac{1}{30}Lp_i \end{bmatrix} \quad (18)$$

Continuing with the solution of Equation (5), we have the inertial force component due to the accelerated motion of the body.

$$M_{ij} = \int_0^L m \frac{\partial^2 \tilde{u}(x,t)}{\partial t^2} \phi_i(x) dx = 0 \quad (19)$$

This equation leads to the mass matrix:

$$M_{ij} = \int_0^L m\, \phi_i(x)\phi_j(x) dx = 0 \quad (20)$$

The mass matrix is then given by:

$$[M_e] = \frac{\rho A L}{420} \begin{bmatrix} 156 & 22L & 54 & -13L \\ 22L & 4L^2 & 13L & -3L^2 \\ 54 & 13L & 156 & -22L \\ -13L & -3L^2 & -22L & 4L^2 \end{bmatrix} \quad (21)$$

3.2 Analysis Including the Effect of Cable Presence

To evaluate the potential contribution of the increased stiffness due to the presence of the prestressing cable, the work associated with the generation of an equivalent transverse distributed force on the beam is analyzed. This force is induced by the moment generated by the prestressing cable when the beam is in a deformed configuration. A concentrically placed cable, subject to axial and vertical constraints at its ends, is considered. The cable is assumed to undergo transverse deformation induced by the deflected shape of the beam, as depicted in Figure 4. Equation (22) presents the variation of the Moment M along the distance x. In this expression, $P(x)$ denotes the axial force along the cable, and $u(x)$ the transverse displacement of the beam. The moment is effectively generated by the horizontal component of $P(x)$, expressed as $P(x)\cos(\alpha)$, with α being the inclination angle of the cable. Under the assumption of a small angle, the approximation $\cos(\alpha) \approx 1$ holds, leading to $P(x)\cos(\alpha) \approx P(x)$.

$$M(x) = P(x)u(x) \quad (22)$$
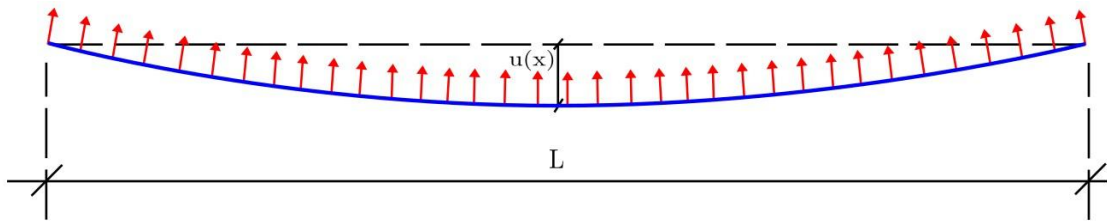
Figure 4 Prestressing force induced by the tendon

Accordingly, the second derivative of the moment defines the equivalent transverse distributed load $w(x)$:

$$\frac{\partial^2 M(x)}{\partial x^2} = w(x) = \frac{\partial^2 P(x)}{\partial x^2}u(x) + 2\frac{\partial P(x)}{\partial x}\frac{\partial u(x)}{\partial x} + P(x)\frac{\partial^2 u(x)}{\partial x^2} \quad (23)$$

Assuming a linear variation of the prestressing force along the beam, as illustrated in Figure 5, the equivalent distributed load is simplified to:

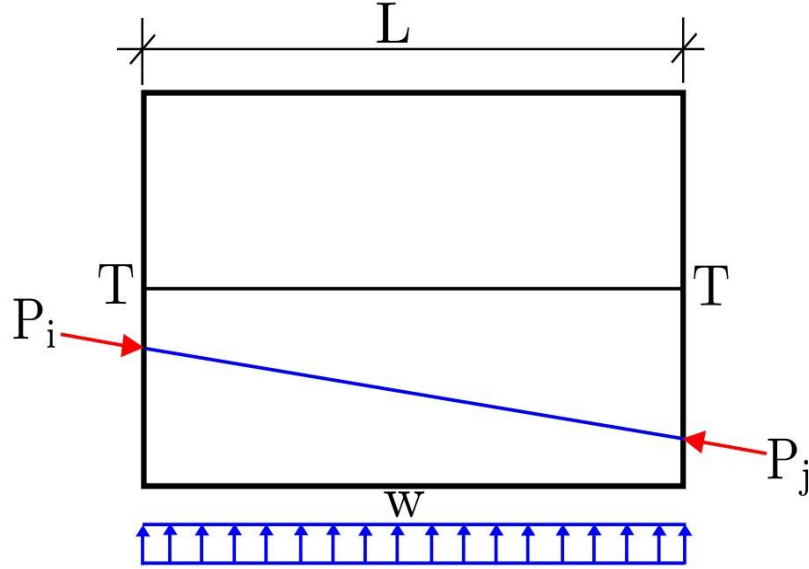$$w(x) = 2\frac{dP(x)}{dx}\frac{du(x)}{dx} + P(x)\frac{d^2u(x)}{dx^2} \quad (24)$$

Figure 5 Linearly varying prestressing force

The mechanical work performed by this equivalent transverse load $w(x)$ is expressed as:

$$\Pi = \int_0^L w(x)u(x)\,dx = \int_0^L [2P'(x)u'(x) + P(x)u''(x)]\,u(x)\,dx \quad (25)$$

Using the finite element approximation $u(x) = \{\phi(x)\}\{\delta\}^T$, the expression for mechanical work becomes:

$$\Pi = \int_0^L [2P'(x)\{\phi'(x)\}\{\delta\}^T + P(x)\{\phi''(x)\}\{\delta\}^T]\,\{\phi(x)\}\{\delta\}^T\,dx \quad (26)$$

The minimization of the total work results in the stiffness matrix associated with the cable contribution:

$$\begin{bmatrix} \dfrac{\delta\Pi}{\delta u_i} \\[2mm] \dfrac{\delta\Pi}{\delta u'_i} \\[2mm] \dfrac{\delta\Pi}{\delta u_j} \\[2mm] \dfrac{\delta\Pi}{\delta u'_j} \end{bmatrix} = [K_{g2}]\begin{bmatrix} u_i \\ u'_i \\ u_j \\ u'_j \end{bmatrix} \quad (27)$$

Each term k_{ij} in the stiffness matrix $[K_{g2}]$ is defined by the following integral:

$$k_{ij} = \int_0^L \phi_j(x)\big(P(x)\,\phi_i{}''(x) + 2P'(x)\,\phi_i{}'(x)\big)dx + \int_0^L \phi_i(x)\Big(P(x)\,\phi_j{}''(x) + 2P'(x)\,\phi_j{}'(x)\Big)dx \quad (28)$$

Upon evaluating the integrals, the stiffness matrix due to the cable is obtained as:

$$[K_{g2}] = \begin{bmatrix} -\frac{1}{5L}(p_j + 11p_i) & -\frac{1}{5}(p_j + p_i) & \frac{6}{5L}(p_j + p_i) & -\frac{1}{5}p_i \\ -\frac{1}{5}(p_j + p_i) & -\frac{1}{15}Lp_j - \frac{1}{5}Lp_i & \frac{1}{5}p_j & \frac{1}{30}L(p_j + p_i) \\ \frac{6}{5L}(p_j + p_i) & \frac{1}{5}p_j & -\frac{1}{5L}(11p_j + p_i) & p_j + \frac{1}{5}p_i \\ -\frac{1}{5}p_i & \frac{1}{30}L(p_j + p_i) & p_j + \frac{1}{5}p_i & -\frac{1}{5}Lp_j - \frac{1}{15}Lp_i \end{bmatrix} \quad (29)$$

3.3 Neutralized Stress State

For the purpose of the modal analysis developed in this study, it is assumed that the beam is in the decompression state of the concrete, which means that the normal stress in the concrete at the level of the prestressing tendons is considered null. This assumption implies that the stresses induced in the concrete by the prestressing forces are fully transferred to the tendons. To ensure this condition, strain compatibility is imposed by equating steel elongation with concrete shortening. This approach is valid in the absence of cracks in the concrete (which is also assumed in this study), and it guarantees that any changes in natural frequencies are only attributed to variations in the prestressing force, without interference from changes in material stiffness.

Consequently, the prestressing force must be defined so that the stress in the centroid of the tendons is annulled, denoted as P_n:

$$P_n = P_p + \Delta P_p \tag{30}$$

where P_p is the applied prestressing force and ΔP_p is the force component required to restore the deformation in the centroid of the tendon. For a discrete finite element model, the initial and final nodal forces i and j are given by the following:

$$(P_n)_i = (P_p)_i + \Delta P_{p_i} \qquad (P_n)_j = (P_p)_j + \Delta P_{p_j} \tag{31}$$

The additional force terms are expressed as:

$$\Delta P_p = \alpha_p A_p (\sigma_{cp})_i \qquad \Delta P_p = \alpha_p A_p (\sigma_{cp})_j \qquad \alpha_p = \frac{E_p}{E_c} \tag{32}$$

where A_p is the cross-sectional area of the tendon and α_p is the modular ratio between steel and concrete. The stress components $(\sigma_{cp})_i$ and $(\sigma_{cp})_j$ at the initial and final ends of the element are defined as:

$$(\sigma_{cp})_i = \frac{(P_p)_i}{A_c} + \frac{(P_p)_i e_i^2}{I_c} + \frac{M_i e_i}{I_c} \qquad (\sigma_{cp})_j = \frac{(P_p)_j}{A_c} + \frac{(P_p)_j e_j^2}{I_c} + \frac{M_j e_j}{I_c} \tag{33}$$

where A_c is the cross-sectional area of the beam, I_c is the moment of inertia and M_i, M_j, e_i, e_j are, respectively, the bending moments due to the self-weight of the beam and the initial and final eccentricities of the tendons. Using these expressions, prestressing forces are incorporated into the stiffness matrices $[K_{g1}]$ and $[K_{g2}]$ to achieve a stress-free state on the tendon centroid, without inducing stress on the surrounding concrete.

3.4 Modal Analysis

The dynamic formulation of the structural system is represented by the matrix equilibrium equation:

$$[\mathbb{M}_e]\ddot{u}(t) + ([K_e] + [K_{g1}] + [K_{g2}])u(t) = F_e(t) \quad (34)$$

where $[\mathbb{M}_e]$ is the mass matrix, $[K_e]$ is the elastic stiffness matrix, $[K_{g1}]$ represents the effect of the axial prestressing force and $[K_{g2}]$ represents the geometric effect associated with the physical presence of the tendon. For the modal analysis, external loads are neglected, that is, $F_e(t) = 0$, and the system's harmonic response is assumed as $u(t) = A\sin(\omega t + \phi)$. Substituting this solution into the equation of motion yields the eigenvalue problem:

$$([K_e] + [K_{g1}] + [K_{g2}] - \omega^2[\mathbb{M}_e])\phi = 0 \quad (35)$$

whose solution provides the natural frequencies ω and the corresponding mode shapes ϕ, incorporating both the prestressing force and the geometric influence of the tendons.

4 NUMERICAL SIMULATIONS OF EXPERIMENTALLY TESTED MODELS

4.1 Description of the validation examples

A total of five experimental studies (Saiidi, Douglas, and Feng 1994; Y. Zhang and Li 2007; Y. T. Zhang, Zheng, and Li 2011; Jang et al. 2011; Noh et al. 2015) investigating the relationship between natural frequencies and prestress losses in beams, previously reported in the literature, were selected to validate the reliability of the finite element model proposed in Section 3. These references encompass a range of geometric configurations and material properties, thereby enabling a comprehensive evaluation of the model's performance under varying conditions. Table 1 provides a comparative summary of the geometric and material parameters associated with each study. For each case, key parameters were extracted, and the experimentally measured fundamental frequencies were compared with those predicted numerically. The analysis of results demonstrated strong agreement between the experimental and numerical values, with relative errors falling within acceptable bounds in most instances. This consistency supports the model's applicability to cases with similar characteristics to those examined in this study.

Table 1 Comparative analysis of geometric and material parameters from different studies.

Parameter	Saiidi et al. (1994)	Zhang and Li (2007)	Zhang et al. (2011)- Beam 1	Zhang et al. (2011)- Beam 2	Jang et al. (2011)	Noh et al. (2015)- Beam 1	Noh et al. (2015)- Beam 2	Noh et al. (2015) - Beam 3
Diameter - φ_p (mm)	12.7	15.2	5.0	5.0	15.2	15.2	15.2	15.2
Base - b (m)	0.102	0.120	0.070	0.077	0.300	0.300	0.300	0.600
Height - h (m)	0.127	0.240	0.140	0.147	0.300	0.300	0.600	0.900
Length - L (m)	3.66	3.90	3.20	3.20	8.00	5.00	10.00	15.00
Number of Cables	1	1	1	1	3	1	1	7
Eccentricity (m)	0.00	0.00	0.00	0.00	0.00	0.00	0.15	Parabolic*

*Eccentricity at mid-span
0.1m and edges at 0.45m

In Table 1, it can be seen that the five studies used to validate the numerical model encompass a wide range of structural configurations. Regarding geometric dimensions, a significant variation was observed between the tested beams, with cross sections ranging from small dimensions, such as 70×140 mm, to more robust beams, with sections of 300×300 mm and 600×900 mm. Regarding the post-tensioning cable configuration, most beams were reinforced with a single cable, except for the studies by Jang et al., who used three cables, and Noh et al., whose experiment involved a parabolic beam with seven cables. The eccentricities applied showed considerable variation between the cases, ranging from cables located in the centroid of the section (null eccentricity) to values of 150 mm. Concerning boundary conditions, all tests were conducted on simply supported beams. More detailed information about the tested beams can be found in the corresponding references.

The process of determining the relationship between the numerical and experimental frequencies when the prestress load varies is divided into two stages. In the first stage, it refers to the calibration of the finite element model for the condition without prestress loads. The natural frequencies were determined through modal analysis, using a discretization of the beam into ten finite elements with three degrees of freedom per node. This level of discretization was verified to be sufficient to ensure the convergence of the first three natural frequencies of the beam. To ensure homogeneity in the analysis of the different cases, the following reference material parameters were adopted as standard values in the absence of specific data: steel density of 7860 kg/m³ and elastic modulus of 210 GPa; concrete density of 2500 kg/m³. Based on this information, the combined density of the concrete and tendons was calculated as the weighted average of the density of each material by its respective volume, divided by the total volume of the beam, according to the following equation:

$$\rho_t = \frac{\rho_c \cdot (A - A_p) \cdot L_b + N_t \cdot \rho_p \cdot A_p \cdot L_t}{A \cdot L_b} \tag{36}$$

where ρ_t is the combined density, ρ_c is the concrete density, A is the cross sectional area of the beam, L_b is the length of the beam, L_t is the length of the tendon, N_t is the number of prestressing tendons, ρ_p is the steel density and A_p is the cross-sectional area of the prestressing tendon, calculated by:

$$A_p = \pi \cdot \left(\frac{\varphi_p}{2}\right)^2 \tag{37}$$

where φ_p is the nominal diameter of the prestressing tendon.

4.2 Computational implementation of the model

The numerical simulations presented in this study were performed using a finite element code entirely developed by the authors in MATLAB. The code follows a modular structure, where each physical or structural component (elements, loads, materials, boundary conditions) is defined through specific functions. The finite element code was organized in the following main stages:

a) **Preprocessing module:** The AddNodes function defines the nodal configuration of the model by assigning spatial coordinates and unique identifiers to each node. The AddElements function establishes the connectivity between nodes, linking each beam element to its corresponding cross-sectional and material properties. The AddCables function enables the modeling of prestressing tendons by specifying their position within the elements, the applied forces, initial and final eccentricities, and the associated section and material parameters. To complement this process, additional functions were implemented to define the structural and loading characteristics of the model. The AddSections function assigns geometric properties such as cross-sectional area and moment of inertia, while the AddMaterials function specifies mechanical properties including the modulus of elasticity and mass density. The AddLoadDT function introduces distributed transverse loads along the beam elements, essential for representing self-weight or other uniformly distributed actions. Lastly, the AddFix function imposes boundary conditions by constraining selected degrees of freedom (translations and rotations) at specific nodes, thereby ensuring appropriate support conditions for the structural system.

b) **Assembly routines:** This stage involves the construction of the global stiffness matrix, which corresponds to the sum of $[K_e]$, $[K_{g1}]$, and $[K_{g2}]$, as indicated in Equation (34), as well as the consistent mass matrix. .

c) **Modal analysis:** Natural frequencies and vibration modes are computed by solving the generalized eigenvalue problem using the assembled mass and global stiffness matrix.

d) **Visualization tools:** The code includes graphical routines for plotting deformed configurations and mode shapes, facilitating the interpretation of structural behavior.

4.3 Calibration of the finite element model without prestress load

The calibration of a finite element model could be formulated as an optimization problem. In this case, the goal is to minimize the error between experimental and numerical natural frequencies for the non-pretensioned beam condition. The objective function is given by:

$$f_{obj} = \frac{1}{N} \sum_{i=1}^{N} \frac{\left| f_{n,i} - f_{n,i}^{\text{exp}} \right|}{f_{n,i}^{\text{exp}}} \tag{38}$$

where $f_{n,i}$ is the ith natural frequency obtained numerically, $f_{n,i}^{\text{exp}}$ is the ith natural frequency measured experimentally, N is the total number of vibration modes considered, and i ranges from 1 to N.

The design variables correspond to the compressive strength of the concrete at 28 days (f_{ck}) for each element in the finite element model for a total of ten variables. For f_{ck}, it is assumed that the range of allowed values is between 2 and 100 MPa. The calibration of the model was carried out using a formulation that, in the absence of experimental data, establishes a relationship between the initial modulus of elasticity (E_{ci}) and f_{ck}. The estimated value of the initial modulus of elasticity is given by the expression (Brazilian Association of Technical Standards 2014):

$$E_{ci} = 5600 \cdot \sqrt{f_{ck}} \tag{39}$$

To solve the optimization problem, the genetic algorithm (GA) available in Matlab (The MathWorks, Inc. 2019) was used. The GA was set up to operate with a population size of 200, running for a maximum of 100 generations. The algorithm was designed to achieve high precision with a tolerance of 1×10^{-8} for the objective function. A summary of the GA parameters and operators is shown in Table 2.

Table 2 Summary of the GA Parameters

Parameter	Value	Description
Population Size	200	Number of individuals in the population
Generations	100	Maximum number of generations
Crossover Function	Heuristic	Crossover function used for recombination
Crossover Fraction	0.9	Fraction of individuals involved in crossover
Elite Count	2	Number of top individuals to be preserved in each generation
Mutation Function	Adaptive Feasible	Mutation function applied to maintain diversity
Creation Function	Uniform	Creation function for initializing the population uniformly
Selection Function	Stochastic Uniform	Selection function for choosing individuals probabilistically

Figure 6 shows a representative example of the results obtained from the optimization of the genetic algorithm, applied to the case study based on the work by Saiidi et al. (1994) (Saiidi, Douglas, and Feng 1994). The parameters used for beam modeling are shown in Table 1 and the two natural frequencies (11.41 Hz and 43.99 Hz). The top plot illustrates the convergence behavior of the algorithm, showing the evolution of the best fitness value and the mean fitness between generations. A rapid decrease in the value of the objective function is observed within the first 20 generations, with the best fitness reaching a value of the order of 10^{-9}, indicating a high level of precision in matching the natural frequencies of the numerical and experimental results. The bottom plot shows the values of the ten optimized characteristic strengths, associated with the elastic moduli as defined by Equation [eq_38], corresponding to each element of the finite element model.
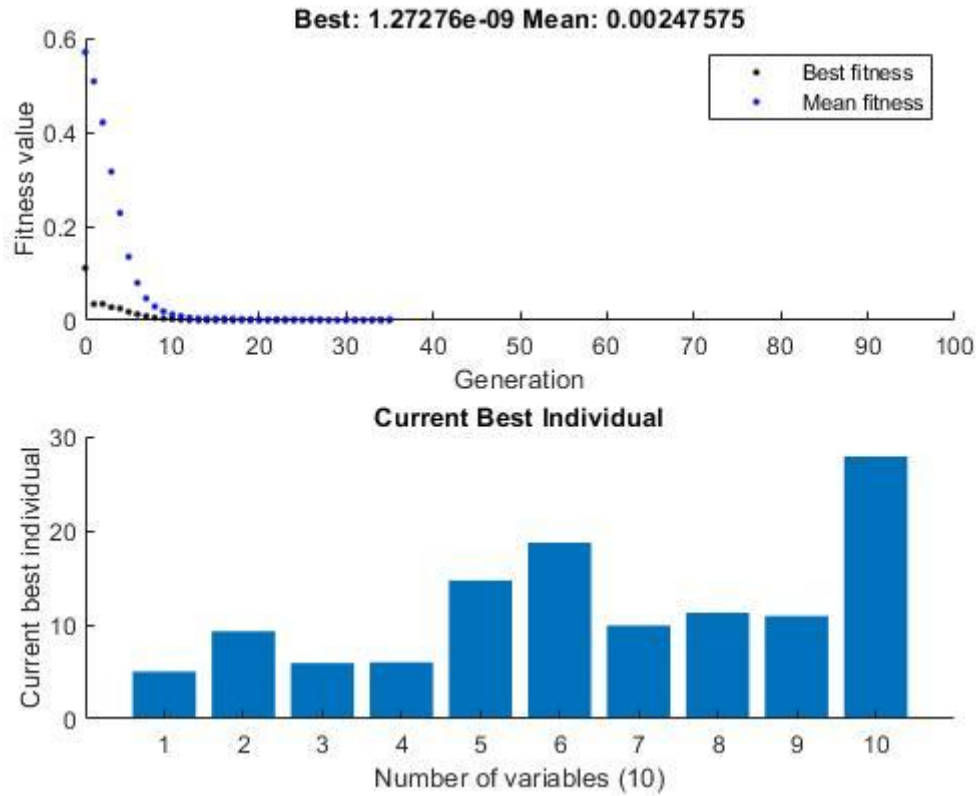
Figure 6 Performance of the genetic algorithm and distribution of optimized characteristic strengths

After this calibration, natural frequencies were simulated for different levels of prestressing force. In the analysis of the experimental data, it is assumed that the prestressing force is uniformly transmitted along the tendon, ignoring possible immediate losses due to friction, anchorage, and concrete shortening.

4.4 Comparison with the tests of Saiidi et al. (1994)

In the free vibration test conducted by Saiidi, Douglas, and Feng (1994), a post-tensioned concrete beam was instrumented with seven accelerometers placed equidistantly along the span to record the dynamic response to impacts applied after different levels of post-tensioning force. For each applied force value, the natural frequencies corresponding to the first and second vibration modes were determined. Table 3 shows a comparison between the experimental results obtained by Saiidi, Douglas, and Feng (1994) and the values predicted by the proposed model for the first two modes. The results indicate that natural frequencies increase gradually with the application of the prestressing force, with the most significant variation occurring in the initial loading stages, taking into account the maximum applied load, equivalent to 56.93% of the critical buckling load of the beam (P_{cr}). The experimental data show a 32.08% increase in the first mode and a 4.02% increase in the second mode, relative to the non-post-tensioning condition.

Table 3 Comparison between the natural frequencies obtained experimentally by Saiidi et al. (1994) and the values estimated by the proposed model.

% Pcr	Prestress Force (kN)	f_1(Hz) Test	f_1(Hz) Model	Error1 (%)	f_2(Hz) Test	f_2(Hz) Model	Error2 (%)
0.00	0.000	11.41	11.41	0.00	43.99	43.99	0.00
11.59	26.732	13.47	12.14	9.84	44.89	44.80	0.20
24.54	56.579	14.15	12.91	8.74	45.71	45.68	0.05
35.07	80.864	14.49	13.51	6.78	45.57	46.39	1.81
52.07	120.051	14.72	14.41	2.09	45.86	47.51	3.60
56.12	129.392	14.97	14.62	2.34	46.10	47.78	3.64

% Pcr	Prestress Force (kN)	f_1(Hz) Test	f_1(Hz) Model	Error1 (%)	f_2(Hz) Test	f_2(Hz) Model	Error2 (%)
56.93	131.261	15.07	14.66	2.71	45.87	47.83	4.27

Similarly, the proposed model predicted increases of 28.49% for the first mode and 8.73% for the second mode, compared to the non-post-tensioning condition. The relative error analysis reveals that the model produced an average error of 5.42% for the first mode and 2.26% for the second mode (excluding the unprestressed case).

4.5 Comparison with Tests by Zhang and Li (2007)

Zhang and Li (2007) investigated the dynamic behavior of a rectangular beam subjected to prestressing using a nonbonded tendon with a linear profile. The natural frequencies obtained experimentally were compared with the results predicted by the proposed model, as presented in Table 4. As in the previous case, the natural frequencies progressively increased with the application of the prestressing force. However, in this experiment, the load levels reached only 3.34% of the critical axial buckling load of the beam, resulting in relatively small variations in the natural frequencies. For the first vibration mode, the experimental results showed an increase of 5.08%, while the model predicted an increase of 1.72% in the same range. In the second mode, the experimental increase was 2.13%, while the model estimated a more modest increase of 0.57%. The average errors between the experimental and predicted frequencies were 2.12% for the first mode and 3.06% for the second. The relatively low level of prestressing compared to the critical load helps explain the modest frequency changes observed, underscoring the system's limited sensitivity to low axial stress levels.

Table 4 Comparison between the natural frequencies obtained experimentally by Zhang and Li (2007) and the values estimated by the proposed model.

% Pcr	Prestress Force (kN)	f_1(Hz) Test	f_1(Hz) Model	Error1 (%)	f_2(Hz) Test	f_2(Hz) Model	Error2 (%)
0.00	0	28.36	28.36	0.00	100.71	100.71	0.00
0.56	20	28.36	28.44	0.29	102.67	100.81	1.82
1.11	40	28.83	28.52	1.06	103.09	100.90	2.12
1.67	60	29.32	28.61	2.44	104.07	101.00	2.95
2.23	80	29.48	28.69	2.69	105.05	101.09	3.77
2.78	100	29.69	28.77	3.10	105.05	101.19	3.68
3.34	120	29.80	28.85	3.19	105.53	101.28	4.02

4.6 Comparison with Tests by Zhang et al. (2011)

Y. T. Zhang, Zheng, and Li (2011) conducted experimental tests on two prestressed concrete beams simply supported. Both beams were prestressed using a straight concentric strand made up of a seven-wire cable with a nominal diameter of 5 mm. Table 5 presents the experimental and numerical results obtained for beam 1, including the natural frequencies of the first three modes at different levels of prestressing force, expressed as a percentage of the critical load (P_{cr}). For Beam 1, the application of up to 22.05% of the critical axial buckling load led to a 6.11% increase in the natural frequency of the first mode in the experimental tests. The proposed model predicted a greater increase of 11.18% for the same mode. In the second and third modes, the experimental frequency increases were 5.73% and 3.78%, respectively, while the model predicted smaller increases of 2.92% and 1.39%. The average errors between the experimental and numerical results were 1.83% for the first mode, 6.46% for the second, and 4.02% for the third.

Table 5 Comparison between the experimental natural frequencies of Zhang et al. (2011) and the values estimated by the proposed model for beam 1

% Pcr	Prestress Force (kN)	f_1(Hz) Test	f_1(Hz) Model	Error1 (%)	f_2(Hz) Test	f_2(Hz) Model	Error2 (%)	f_3(Hz) Test	f_3(Hz) Model	Error2 (%)
0.00	0.0	19.14	19.14	0.00	76.66	76.66	0.00	167.96	167.96	0.00
2.13	7.9	19.30	19.36	0.30	78.70	76.88	2.31	168.57	168.19	0.23
8.90	33.0	19.92	20.03	0.57	84.96	77.57	8.70	174.31	168.90	3.10
13.63	50.5	20.31	20.49	0.89	87.40	78.05	10.70	173.34	169.40	2.27
19.43	72.0	20.50	21.04	2.64	85.44	78.64	7.96	160.64	170.01	5.84
22.05	81.7	20.31	21.28	4.79	81.05	78.90	2.65	156.73	170.29	8.65

Table 6 provides the data related to beam 2, allowing for a further comparative evaluation. For beam 2, the mean errors between the experimental results and those predicted by the proposed model remained below 2% for the first mode. An increase in prestressing force from 0% to 15.60% of the critical load led to a 9.70% increase in the natural experimental frequency of the first mode, while the model predicted an increase of 7.64%. For higher-order modes, the variations were significantly smaller, with increases of only 5.30% and 1.30% for the second and third modes, respectively.

Table 6 Comparison between the experimental natural frequencies of Zhang et al. (2011) and the values estimated by the proposed model for beam 2

% Pcr	Prestress Force (kN)	f_1(Hz) Test	f_1(Hz) Model	Error1 (%)	f_2(Hz) Test	f_2(Hz) Model	Error2 (%)	f_3(Hz) Test	f_3(Hz) Model	Error2 (%)
0.00	0	22.07	22.07	0.00	83.00	83.00	0.00	150.39	150.39	0.00
3.54	20	22.65	22.46	0.82	83.49	83.53	0.05	151.36	151.07	0.19
7.09	40	22.85	22.85	0.01	85.44	84.05	1.63	148.43	151.74	2.23
10.63	60	23.63	23.23	1.68	86.91	84.57	2.69	152.46	152.41	0.03
14.18	80	24.02	23.61	1.72	87.89	85.08	3.20	154.29	153.07	0.79
15.60	88	24.21	23.76	1.88	87.40	85.29	2.42	148.43	153.34	3.31

In general, the results indicate that for both tested beams, the natural frequencies increased as a function of the applied prestressing force. The proposed model proved effective in estimating the frequencies, particularly for the first vibration mode, with errors consistently below 4%. However, the accuracy of the model decreases for higher-order modes, with a greater dispersion observed in the results. It should be noted that, as shown in Table 5 and 6 , the natural frequencies in some situations exhibited a decrease at the final loading level compared to the value obtained at the previous level. This behavior, which deviates from the expected trend, could not be explained by the proposed model, and it was not possible to determine whether it was the result of an experimental inconsistency or an anomaly in the data acquisition process.

4.7 Comparison with Tests by Jang et al. (2011)

Jang et al. (2011) conducted experimental tests on a total of six post-tensioned concrete beams, each subjected to a distinct prestressing force. The beams were longitudinally reinforced with four 16 mm diameter steel bars and 10 mm diameter transverse stirrups, arranged with spacing varying between 100 and 150 mm. For prestressing, three straight and concentric tendons, each 15.2 mm in diameter, were used. Table 7 shows the natural frequencies obtained experimentally for the first and second modes of vibration, along with the values estimated by the proposed finite element model, allowing for a comparative analysis between both sets of results. For the first mode, an increase of 17.05% in the experimental natural frequency was observed as the prestressing force increased to 15.81% of the critical load. The proposed model estimated an increase of 21.77% for the same interval. For the second mode, the variation observed in the experimental results was 5.30%.

Table 7 Comparison between the natural frequencies obtained experimentally by Jang et al. (2011) and the values estimated by the proposed model.

% Pcr	Prestress Force (kN)	f_1(Hz) Test	f_1(Hz) Model	Error1 (%)	f_2(Hz) Test	f_2(Hz) Model	Error2 (%)
0.00	0	7.51	7.51	0.00	28.18	28.18	0.00
4.41	146	8.21	8.00	2.56	29.39	28.72	2.26
7.98	264	8.53	8.38	1.81	30.97	29.16	5.85
10.76	356	8.72	8.66	0.73	29.99	29.49	1.66
14.06	465	8.69	8.98	3.32	30.12	29.88	0.80
15.81	523	8.79	9.14	4.04	29.85	30.09	0.79

Taking into account the difference between the values obtained for the first and last loadings, the smallest discrepancy between the numerical and experimental results occurred for the first mode at intermediate loading (10.76% of P_{cr}), with an error of only 0.73%. For the second mode, the largest relative error was 5.85%. In addition, one relevant aspect is that the methodology adopted involved applying a single prestressing force per beam, without prior measurement of the natural frequencies in the unprestressed state. Thus, for the implementation of the numerical model, it was assumed

that all beams were structurally identical in the initial state, which may have introduced uncertainties in the results. However, the calculated values were in good agreement with the experimental results.

4.8 Comparison with Tests by Noh et al. (2015)

According to Noh et al. (2015), several factors influence the natural frequency of post-tensioned concrete beams, including the level of prestressing force, the location and profile of the tendon, boundary conditions, and concrete shrinkage, among others. However, a simultaneous experimental analysis of all these variables is not feasible. Therefore, the study conducted by the authors focused on three main parameters: the level of prestressing, the position of the tendon, and its geometric profile. In the laboratory experiment, three different beams were tested, each with a different prestressing configuration: a straight tendon without eccentricity, a straight tendon with eccentricity, and a tendon with a parabolic profile. The tendons, with a nominal diameter of 15.2 mm, were tensioned at four different levels of prestressing force. The dynamic response was recorded using four accelerometers, allowing the extraction of the natural frequencies of the first two vibration modes.

Tables 8, 9, and 10 show, respectively, the applied prestressing force values, the experimental and numerical natural frequencies, and the relative errors for the three mentioned configurations. Although the stated objective of the study by Noh et al. (2015) was to compare the effects of the tendon profiles on the natural frequencies of post-tensioned concrete beams, the samples tested exhibited different geometric dimensions. This variation prevents a direct and proportional comparison of the influence of eccentricity, making it difficult to isolate the impact of the tendon profile on the dynamic response. However, the results obtained allow for the identification of trends consistent with previous studies discussed in this work. Regarding the precision of the numerical model, the lowest average errors were observed for the second mode, with a mean discrepancy of 2.27%, compared to 2.49% for the first mode (excluding the unprestressed case). This indicates that the model was slightly more consistent in predicting the second vibration mode.

Table 8 Comparison between the natural frequencies obtained experimentally by Noh et al. (2015) and the values estimated by the proposed model (straight tendon without eccentricity).

% Pcr	Prestress Force (kN)	f_1(Hz) Test	f_1(Hz) Model	Error1 (%)	f_2(Hz) Test	f_2(Hz) Model	Error2 (%)
0.00	0	20.51	20.51	0.00	77.76	77.76	0.00
2.86	272	20.39	20.80	2.03	79.10	78.07	1.30
5.71	544	20.51	21.10	2.85	77.45	78.39	1.21
8.57	816	20.51	21.38	4.25	79.53	78.70	1.04
11.42	1088	20.57	21.66	5.32	77.82	79.01	1.53

Table 9 Comparison between the natural frequencies obtained experimentally by Noh et al. (2015) and the values estimated by the proposed model (straight tendon with eccentricity).

% Pcr	Prestress Force (kN)	f_1(Hz) Test	f_1(Hz) Model	Error1 (%)	f_2(Hz) Test	f_2(Hz) Model	Error2 (%)
0.00	0	9.16	9.16	0.00	30.76	30.76	0.00
1.80	272	9.22	9.25	0.27	30.82	30.87	0.15
3.59	544	9.28	9.33	0.54	31.25	30.97	0.89
5.39	816	9.28	9.41	1.44	31.25	31.08	0.56
7.18	1088	9.28	9.50	2.33	31.31	31.18	0.42

Table 10 Comparison between the natural frequencies obtained experimentally by Noh et al. (2015) and the values estimated by the proposed model (tendon with parabolic profile)

% Pcr	Prestress Force (kN)	f_1(Hz) Test	f_1(Hz) Model	Error1 (%)	f_2(Hz) Test	f_2(Hz) Model	Error2 (%)
0.00	0	5.86	5.86	0.00	22.22	22.22	0.00
0.65	272	5.86	5.99	2.27	22.22	22.36	0.64
1.30	544	6.10	6.12	0.38	23.19	22.50	2.96
1.95	816	6.35	6.25	1.56	23.68	22.64	4.38
2.60	1088	6.35	6.38	0.40	23.68	22.78	3.79

5 DISCUSSIONS OF RESULTS

Figures 7 and 8 compare numerical (FEM) and experimental (EXP) results for the analyzed beams under axial compressive loads ranging as a percentage of the critical load (%Pcr) ,for Modes 1 and 2, respectively.The results of the five experimental studies consistently demonstrate an increase in natural frequencies with the application of prestressing force. In all cases, prestressing led to an upward shift in the natural frequencies, most notably in the fundamental (first) vibration mode. This behavior is consistent with theoretical expectations for prestressed concrete structures, where axial compression enhances the effective stiffness. The increase rate was most significant in the first mode, which is generally more responsive to stiffness variations. In contrast, higher-order modes exhibited comparatively smaller changes, suggesting that prestressing has a more pronounced influence on the fundamental frequency than on higher modes. In particular, some studies reported anomalous decreases in frequency during the final stages of loading, a trend not captured by the proposed model. These deviations may be attributed to experimental uncertainties or unmodeled phenomena such as microcracking and abrupt prestress losses, which are not incorporated into the current model formulation.
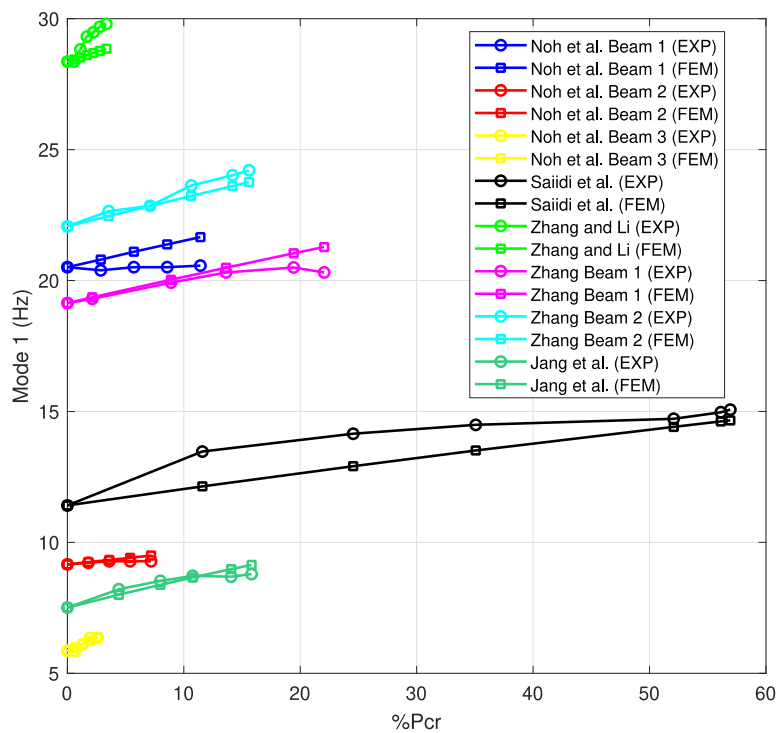
Figure 7 Comparison of Mode 1 as a function of Load Ratio (%Pcr) between experimental (EXP) and numerical model (FEM)
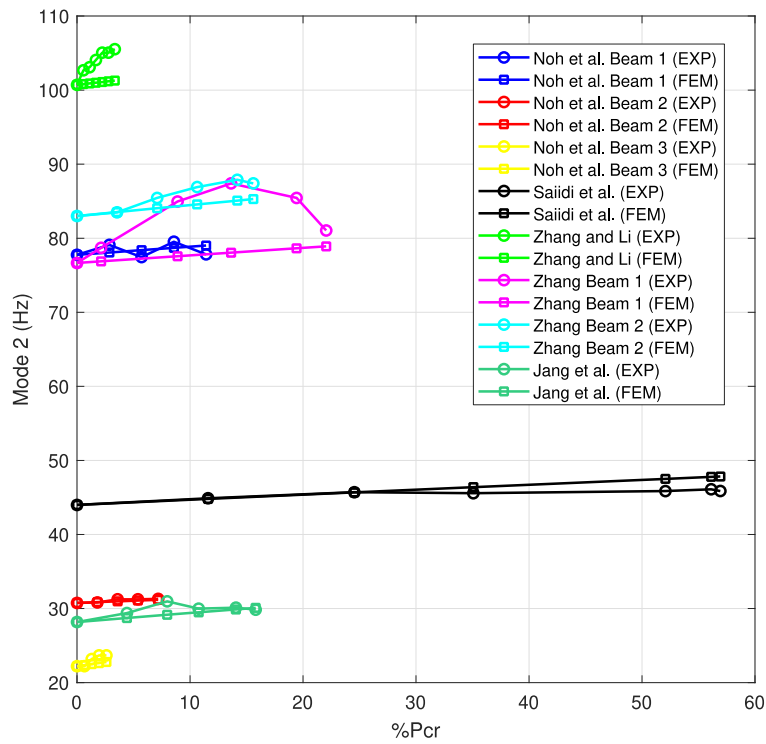
Figure 8 Comparison of Mode 2 as a function of Load Ratio (%Pcr) between experimental (EXP) and numerical model (FEM)

The proposed model demonstrates high accuracy under low to medium axial load levels, up to approximately 15% of the critical load, with errors consistently remaining below 3%. It also exhibits strong generalizability in varying structural geometries and tendon profiles, maintaining robust performance even in experimental setups involving load eccentricities and parabolic tendon configurations. Table 11 summarizes the mean absolute errors between the experimental frequencies and the numerically predicted frequencies for the first modes.

Table 11 Mean absolute errors

Study	Mode 1 (%)	Mode 2 (%)	Mode 3 (%)
Saiidi et al. (1994)	5.42	2.26	-
Zhang and Li (2007)	2.13	3.06	-
Zhang et al. (2011) Beam 1	1.83	6.46	4.02
Zhang et al. (2011) Beam 2	1.22	2.00	1.31
Jang et al. (2011)	2.49	2.27	-
Noh et al. (2015) Straight Tendon without Eccentricity	3.62	1.27	-
Noh et al. (2015) Straight Tendon with Eccentricity	1.15	0.5	-
Noh et al. (2015) Parabolic Tendon	1.16	2.94	-

The analysis of global errors indicates that the model performs satisfactorily in predicting natural frequencies, particularly for the first two modes. For Mode 1, the global average error was 2.48%, while for Mode 2 it was 2.62%. Although the average values are similar, the variability index reveals a difference in the consistency of the results: 0.88 for Mode 1, indicating a greater dispersion of errors between studies, and 0.68 for Mode 2, suggesting a more uniform performance. The comparative analysis of the five studies confirms that the proposed model demonstrates high robustness in estimating the natural frequencies of post-tensioned beams, especially under moderate axial load levels. Although

limitations exist, particularly at high loads, the results indicate that the numerical formulation is adequate for practical engineering applications.

6 CONCLUSIONS

This study aimed to evaluate the influence of prestressing force on the dynamic behavior of prestressed concrete beams, accounting for both the axial load effect and the physical presence of tendons. Through the analysis of experimental data from existing literature and numerical simulations performed using the finite element model developed herein, the study provides insights that advance the understanding and modeling of this phenomenon.

An increase in natural frequency was observed with the application of prestressing force, primarily due to the stiffening effect induced by the physical presence of the tendon—an effect found to be more influential than that of axial load alone. This increase was more pronounced in the lower vibration modes and became less significant in higher modes. Numerical simulations revealed that the greatest frequency gains occurred during the initial stages of loading, tending to stabilize as the prestressing force approached the critical threshold. The proposed model demonstrated strong accuracy in predicting natural frequencies, particularly for the first two modes, with average errors of 2.48% and 2.68% for the first and second modes, respectively.

The model's simple formulation and ease of computational implementation make it well-suited for integration into structural design processes and optimization routines. These features, combined with their low computational cost, indicate strong potential for practical engineering applications requiring efficient yet reliable dynamic assessments. Based on the findings, it is recommended that future research incorporates modeling of immediate prestress losses, as these may affect the dynamic response and enhance the model's accuracy. Overall, the proposed model offers a promising tool for evaluating the structural integrity of prestressed beams via dynamic monitoring. When supplemented with visual inspections, such assessments can support the validation of prestress losses and inform decisions related to design, maintenance, and rehabilitation strategies.

Acknowledgments

List of Symbols

A Cross-sectional area of the beam (m^2)

Ap Cross-sectional area of the prestressing tendon (m^2)

E Elastic modulus of the beam material (Pa)

Ep Elastic modulus of the prestressing tendon (Pa)

Ec Elastic modulus of the concrete (Pa)

EI Flexural rigidity (N·m^2)

f_n Natural frequency at mode n (Hz)

f_{ck} Characteristic compressive strength of concrete (MPa)

I Moment of inertia of the cross section (m^4)

L Length of the beam (m)

M Bending moment (N·m)

m Mass per unit length (kg/m)

Me Mass matrix

N Axial compressive force (N)

$P, P(x)$ Prestressing force as a function of position (N)

Pcr Critical buckling load (N)

Pn Neutral prestressing force (N)

Pp Applied prestressing force (N)

$q(x, t)$ Transverse distributed load (N/m)

ρ Material density (kg/m^2)

$ρ_t$ Total (combined) density of the system (kg/m^3)

$ω_n$ Angular frequency at mode n (rad/s)

$u(x, t)$ Transverse displacement at position x and time t

$ϕ_i(x)$ Shape function associated with node i

$α_p$ Modular ratio (E_p/E_c)

e Eccentricity of the prestressing tendon (m)

$ΔP_p$ Additional force to restore tendon strain (N)

$Kg1$ Geometric stiffness matrix due to axial prestress

$Kg2$ Geometric stiffness matrix due to tendon profile effect

Ke Elastic stiffness matrix

V Shear force (N)

References

Abdel-Jaber, Hiba, and Branko Glisic. 2019. "Monitoring of Prestressing Forces in Prestressed Concrete Structures—an Overview." *Structural Control and Health Monitoring* 26 (6): e2374. https://doi.org/10.1002/stc.2374.

Amir, Oded, and Emad Shakour. 2018. "Simultaneous Shape and Topology Optimization of Prestressed Concrete Beams." *Structural and Multidisciplinary Optimization* 57 (5): 1831–43. https://doi.org/10.1007/s00158-017-1855-5.

Bai-Jian, Tang, Wang Fei, and Chen Song. 2018. "Effect of Prestress Force on Natural Bending Frequency of External Prestressed Steel Beams." *The Open Civil Engineering Journal* 12 (1): 62–70. https://doi.org/10.2174/1874149501812010062.

Bao, Y., Z. Chen, H. Li, and Y. L. Xu. 2021. "Deep Learning-Based Damage Detection for Prestressed Concrete Beams Using Dynamic Response Data." *Automation in Construction* 122: 103470.

Bokai, A. 1988. "Natural Frequencies of Beams Under Compressive Axial Loads." *Journal of Sound and Vibration* 126 (1): 49–65.

Bokaian, A. 1988. "Natural Frequencies of Beams Under Compressive Axial Loads." *Journal of Sound and Vibration* 126 (1): 49–65.

Bonopera, Marco, Kuo-Chun Chang, and Zheng-Kuan Lee. 2020. "State-of-the-Art Review on Determining Prestress Losses in Prestressed Concrete Girders." *Applied Sciences* 10 (20): 7257. https://doi.org/10.3390/app10207257.

Bonopera, M., K. C. Chang, C. C. Chen, Y. C. Sung, and N. Tullini. 2019. "Experimental Study on the Fundamental Frequency of Prestressed Concrete Bridge Beams with Parabolic Unbonded Tendons." *Journal of Sound and Vibration*. https://doi.org/https://doi.org/10.1016/j.jsv.2019.04.038.

Brazilian Association of Technical Standards. 2014. "NBR 6118: Design of concrete structures — Procedure." Rio de Janeiro: ABNT.

Breccolotti, Marco. 2018. "On the Evaluation of Prestress Loss in PRC Beams." *International Journal of Concrete Structures and Materials* 12.

Choudhary, M. P., and S. S. Sanghai. 2019. "Pre-Stressed Concrete Bridge Girder Analysis, Design & Optimization - a Review." *International Journal for Research in Applied Science & Engineering Technology (IJRASET)* 7 (4): 1786–90. https://doi.org/10.22214/ijraset.2019.4324.

Cook, Robert D., David S. Malkus, Michael E. Plesha, and Robert J. Witt. 2002. *Concepts and Applications of Finite Element Analysis*. 4th ed. New York: John Wiley & Sons.

Dall'Asta, A., and L. Dezi. 1996. "Discussion of 'Prestress Force Effect on Vibration Frequency of Concrete Bridges' by m. Saiidi, b. Douglas, and s. Feng." *Journal of Structural Engineering* 122 (4): 458–58. https://doi.org/10.1061/(asce)0733-9445(1996)122:4(458).

Deak, G. 1996. "Discussion of 'Prestress Force Effect on Vibration Frequency of Concrete Bridges' by m. Saiidi, b. Douglas, and s. Feng." *Journal of Structural Engineering* 122 (4): 458–59. https://doi.org/10.1061/(asce)0733-9445(1996)122:4(458).

Fleischman, Robert B., and Kim Seeber. 2016. "New Construction for Resilient Cities: The Argument for Sustainable Low Damage Precast/Prestressed Concrete Building Structures in the 21st Century." *Scientia Iranica* 23 (4): 1578–93. https://doi.org/10.24200/sci.2016.2230.

Gan, Bing-zheng, Sing-ping Chiew, Yong Lu, and Tat-ching Fung. 2019. "The Effect of Prestressing Force on Natural Frequencies of Concrete Beams – a Numerical Validation of Existing Experiments by Modelling Shrinkage Crack Closure." *Journal of Sound and Vibration* 455: 20–31. https://doi.org/10.1016/j.jsv.2019.04.030.

Hamed, Ehab, and Y. Frostig. 2006. "Natural Frequencies of Bonded and Unbonded Prestressed Beams–Prestress Force Effects." *Journal of Sound and Vibration* 295 (1-2): 28–39. https://doi.org/10.1016/j.jsv.2005.11.032.

Hop, Tong. 1991. "The Effect of Degree of Prestressing and Age of Concrete Beams on Frequency and Damping of Their Free Vibration." *Materials and Structures* 24 (3): 210–20. https://doi.org/10.1007/bf02472987.

Jahjouh, Mahmoud, and Semih Erhan. 2022. "Optimization of Prestressed Concrete Bridge Girder Section Using a Modified Harmony Search Algorithm." *Structures* 46: 625–36. https://doi.org/10.1016/j.istruc.2022.10.093.

Jain, S. K., and S. C. Goel. 1996. "Discussion of 'Prestress Force Effect on Vibration Frequency of Concrete Bridges' by m. Saiidi, b. Douglas, and s. Feng." *Journal of Structural Engineering* 122 (4): 459–60. https://doi.org/10.1061/(asce)0733-9445(1996)122:4(458).

Jaiswal, Omprakash. 2008. "Effect of Prestressing on the First Flexural Natural Frequency of Beams." *Structural Engineering and Mechanics* 28 (5): 515–24. https://doi.org/10.12989/sem.2008.28.5.515.

Jang, Jung-bum, Hong-pyo Lee, Kyeong-min Hwang, and Young-chul Song. 2011. "Prediction of Prestress Force on Grouted Tendon by Experimental Modal Analysis." In *Dynamics of Civil Structures, Volume 4*, 33–39. Springer New York. https://doi.org/10.1007/978-1-4419-9831-6_5.

Kim, Hyeong-Tag, Hyung-Joon Seo, and In-Hwan Yang. 2019. "Application of Partial Prestressing for Crack Control in PSC Cylinder Members." In *AIP Conference Proceedings*, 2158:020027. 1. AIP Publishing. https://doi.org/10.1063/1.5127610.

Kim, Jeong-Tae, Yeon-sun Ryu, and Chung-bang Yun. 2003. "Vibration-Based Method to Detect Prestress Loss in Beam-Type Bridges." In *Smart Structures and Materials 2003: Smart Systems and Nondestructive Evaluation for Civil Infrastructures*, 559–68. SPIE. https://doi.org/10.1117/12.484638.

Kovalovs, Andrejs, Sandris Ručevskis, Pavel Akishin, and J. Kolupajevs. 2017. "Numerical Investigation on Detection of Prestress Losses in a Prestressed Concrete Slab by Modal Analysis."

Law, S. S., and Z. R. Lu. 2005. "Time Domain Responses of a Prestressed Beam and Prestress Identification." *Journal of Sound and Vibration* 288 (4-5): 1011–25. https://doi.org/10.1016/j.jsv.2005.01.045.

Li, Jie, and Feng Zhang. 2016. "Experimental Research and Numerical Simulation of Influence of Pre-Stress Values on the Natural Vibration Frequency of Concrete Simply Supported Beams." *Journal of Vibroengineering* 18 (7): 4592–4604. https://doi.org/10.21595/jve.2016.17196.

Liu, Y., Y. Zhang, Z. Chen, and X. Wang. 2022. "Smart Sensing and Health Monitoring of Prestressed Concrete Bridges: A Review." *Sensors* 22 (12): 4511.
Lu, Z. R., and S. S. Law. 2006. "Identification of Prestress Force from Measured Structural Responses." *Mechanical Systems and Signal Processing* 20 (8): 2186–99. https://doi.org/10.1016/j.ymssp.2005.09.001.

Mamandi, Ahmad, Mohammad H. Kargarnovin, and Salman Farsi. 2012. "Dynamic Analysis of a Simply Supported Beam Resting on a Nonlinear Elastic Foundation Under Compressive Axial Load Using Nonlinear Normal Modes Techniques Under Three-to-One Internal Resonance Condition." *Nonlinear Dynamics* 70 (2): 1147–72. https://doi.org/10.1007/s11071-012-0520-1.

Miyamoto, Ayaho, Katsuji Tei, Hideaki Nakamura, and John W. Bull. 2000. "Behavior of Prestressed Beam Strengthened with External Tendons." *Journal of Structural Engineering* 126 (9): 1033–44. https://doi.org/10.1061/(asce)0733-9445(2000)126:9(1033).

Noble, Darragh, Maria Nogal, Alan O'Connor, and Vikram Pakrashi. 2016. "The Effect of Prestress Force Magnitude and Eccentricity on the Natural Bending Frequencies of Uncracked Prestressed Concrete Beams." *Journal of Sound and Vibration* 365: 22–44. https://doi.org/10.1016/j.jsv.2015.11.047.

Noble, Darragh, Alan O'Connor, María Nogal, and Vikram Pakrashi. 2014. "The Effect of Prestress Force Magnitude on the Natural Bending Frequencies of Prestressed Concrete Structures." In *23rd Australasian Conference on the Mechanics of Structures and Materials (ACMSM23)*, 333–38.

Noh, Myung-Hyu, Taek-Ryong Seong, Jungwhee Lee, and Kyu-Sik Park. 2015. "Experimental Investigation of Dynamic Behavior of Prestressed Girders with Internal Tendons." *International Journal of Steel Structures* 15 (2): 401–14.

Raju, K. Kanaka, and G. Venkateswara Rao. 1986. "Free Vibration Behavior of Prestressed Beams." *Journal of Structural Engineering* 112 (2): 433–37. https://doi.org/10.1061/(asce)0733-9445(1986)112:2(433).

Ribeiro, D., R. Calçada, M. Brehm, and H. Müller. 2021. "Machine Learning Techniques for Monitoring Prestressed Concrete Bridges." *Engineering Structures* 244: 112772.

Risan, Hussam K., and Rana I. K. Zaki. 2022. "Meta-Analysis for Influence of Prestress Force on the Natural Frequency and Prestress Loss of Concrete Member." *European Journal of Engineering and Technology Research* 7 (1): 90–94. https://www.ej-eng.org/index.php/ejeng/article/view/2574.

Saidin, Siti Shahirah, Adiza Jamadin, Sakhiah Abdul Kudus, Norliyati Mohd Amin, and Muhamad Azhan Anuar. 2022. "An Overview: The Application of Vibration-Based Techniques in Bridge Structural Health Monitoring." *International Journal of Concrete Structures and Materials* 16 (1): 69. https://doi.org/10.1186/s40069-022-00557-1.

Saiidi, Mehdi Saiid, Bruce M. Douglas, and Shaoshuai Feng. 1994. "Prestress Force Effect on Vibration Frequency of Concrete Bridges." *Journal of Structural Engineering* 120: 2233–41. https://doi.org/10.1061/(ASCE)0733-9445(1994)120:7(2233).

Shaker, Francis J. 1975. "Effect of Axial Load on Mode Shapes and Frequencies of Beams." Vol. 8109. NASA Lewis Research Centre Report.

Shakur, Emad, Adaya Shaked, and Oded Amir. 2024. "Topology and Shape Optimization of 3D Prestressed Concrete Structures." *Engineering Structures* 321: 118936. https://doi.org/10.1016/j.engstruct.2024.118936.

Shi, Luning, Haoxiang He, and Weiming Yan. 2014. "Prestress Force Identification for Externally Prestressed Concrete Beam Based on Frequency Equation and Measured Frequencies." *Mathematical Problems in Engineering* 2014: 1–13. https://doi.org/10.1155/2014/840937.

The MathWorks, Inc. 2019. *MATLAB Version R2019b*. Natick, Massachusetts, United States: The MathWorks, Inc.

Vibhute, Aditi S., Poonam Kotulkar, Trupti Kshirsagar, and Prachity Janrao. 2016. "Analysis of Natural Frequency of Prestressed Steel Beam with Triangular Tendon Profile." *International Research Journal of Engineering and Technology (IRJET)*, 701–6.

Wang, L., H. Li, and Y. L. Xu. 2020. "Enhanced Modal Identification of Prestressed Beams via Advanced Signal Processing." *Mechanical Systems and Signal Processing* 144: 106875.

Wang, Ta-heng, Ran Huang, and Tz-wei Wang. 2013. "The Variation of Flexural Rigidity for Post-Tensioned Prestressed Concrete Beams." *Journal of Marine Science and Technology*, 300–308.

Zanini, Mariano Angelo, Flora Faleschini, and Carlo Pellegrino. 2022. "New Trends in Assessing the Prestress Loss in Post-Tensioned Concrete Bridges." *Frontiers in Built Environment* 8: 956066. https://doi.org/10.3389/fbuil.2022.956066.

Zhang, Yao Ting, Yi Zheng, and Hong Jian Li. 2011. "A Dynamic Test of Fully Prestressed Concrete Beams." *Advanced Materials Research* 368-373: 2483–90. https://doi.org/10.4028/www.scientific.net/amr.368-373.2483.

Zhang, Y., and R. Li. 2007. "Natural Frequency of Full-Prestressed Concrete Beam." *Transactions of Tianjin University* 13 (5): 354–59.

Zhao, Xiao, and Hongqiang Fang. 2012. "Analysis of Cable Force Loss of Prestressing Structure During Tension Construction." *Progress in Structure, Pts 1-4* 166-169: 809–14.

Zhou, Y., H. Li, and X. Zhang. 2020. "Effects of Tendon Eccentricity on Dynamic Responses of Prestressed Beams." *Journal of Bridge Engineering* 25 (8): 04020048.

Zienkiewicz, O. C., R. L. Taylor, and J. Z. Zhu. 2013. *The Finite Element Method: Its Basis and Fundamentals*. 7th ed. Oxford: Butterworth-Heinemann. https://doi.org/10.1016/C2009-0-24909-9.